Energy Yield Prediction of a Bifacial PV System with a Miniaturized Test Array

Hartmut Nussbaumer[+], Markus Klenk*, Marco Morf and Nicolas Keller

Zurich University of Applied Science, SoE, Institute of Energy Systems and Fluid Engineering

Technikumstrasse 9, 8401 Winterthur, Switzerland

[+]phone: +41 58 934 4799, [+]e-mail: hartmut.nussbaumer@zhaw.ch

*phone: +41 58 934 4804, *e-mail: markus.klenk@zhaw.ch (corresponding author)

Abstract - Because of the sensitivity on multiple additional factors, compared to monofacial standard installations, the simulation and prediction of a bifacial PV arrays yield is by far more complicated and less reliable. Accordingly, the determination of optimized installation conditions is considerably less straightforward for bifacial installations. Due to the pronounced dependencies also the assignability of otherwise applied installation conditions to similar systems is limited.

Because of the low accuracy of the traditional approaches to predict the bifacial system output the use of a miniaturized test rig might be an interesting option. Provided that the results can be assigned to measurements at real systems it can be used as a cheap and flexible testing device. Miniaturized devices could be used in long-term trials for yield measurements at specific locations, to identify optimum installation conditions or to validate simulation algorithms. Running several test rigs with different configurations in parallel would enable a direct comparison. The small size of a miniaturized rig also allows a fast change of the set-up, which is an interesting feature to test the respective impact at otherwise almost unchanged conditions in short-term tests.

In this paper we report on a test device which is a miniaturized (1:12) replica of an existing PV array with commercial bifacial modules. The measurement data of both systems are compared in order to investigate if there is a clear assignability. A unique feature of the large test field, a permanent and automated variation of the tilt angle, is also transferred to the miniaturized version. Accordingly, the whole tilt angle range is tested and potential tilt angle dependent effects are revealed. Based on the obtained data we give an estimation of the error in the prediction accuracy and discuss options for possible improvements.

Keywords: Bifacial, Energy yield prediction, Test system, Tilt angle

1. Introduction

A major motivation for bifacial PV is an expected additional power yield, compared to monofacial panels, due to the two sided light sensitivity. Bifaciality also enables interesting opportunities, such as a broadening of the energy generation profile or alternative mounting concepts.(Guerrero-Lemus et al., 2016; Kopecek and Libal, 2018).

Due to technical progress, such as improved bifacial cell concepts or the availability of thin solar glass, the technology gets increasingly attractive. Also, some of the innovative solar cell technologies, which are currently implemented in industrial production, allow a comparatively simple adaption to a bifacial lay-out (Buchholz et al., 2017; Colville, 2017; Kopecek et al., 2015; Teppe et al., 2015). The general trend towards glass/glass-modules with superior reliability, as well as the interest in “peak shaving” and customized solutions for specific applications (Obara et al., 2014; Faturrochman et al., 2018; Soria et al., 2016), further supports the development towards bifacial technology. The potential for an improved module power output was repeatedly demonstrated by simulations and measurements on single modules or installations in various orientations and for various locations (Castillo-Aguilella and Hauser, 2016; Chiodetti, 2015; Guo et al., 2013; Kopecek and Libal, 2018; Kreinin et al., 2011; Shoukry et al., 2016; Stein et al., 2017; Sugibuchi et al., 2013; Sun et al., 2018).

In spite of the advantages of bifacial PV systems there was no real breakthrough in terms of the installed capacity up to now (ITRPV roadmap, 2018). This is mainly due to the limited yield predictability by the available means, which is a major obstacle with regard to the bankability (Colville, 2018; Foehringer Merchant, 2018; Osborne, 2017; Richter, 2018; Romero and Kedir, 2018).

Due to the two-sided sensitivity of bifacial modules additional factors, compared to a standard monofacial PV module, such as the ground reflectivity, rear side irradiation homogeneity or the installation height need to be considered. In real, extended PV systems the complexity is again increased due to mutual shading of adjacent module rows in form of direct shading of modules and because of a reduced albedo from the ground. Bifaciality also enables unconventional mounting options such as vertical installation, which again cause different irradiation and shading conditions, compared to conventional systems.

The increased complexity results in a considerable uncertainty concerning the yield expectation of projected PV systems or the actual benefit due to bifaciality. Numerous publications report on the measured bifacial gain of real systems (Joanny et al., 2017; Kopecek and Libal, 2018) to reveal the typical range which can be expected. For a quantitative appraisal however a further development of simulation tools for bifacial systems is necessary.

While the use of simulation tools is state-of-the-art and widely accepted to calculate the yield of projected monofacial standard systems, their adaption for bifacial systems is still ongoing and their reliability needs to be proven by comparison with measured data. The lack of suitable simulation tools also hinders the definition of the optimum installation conditions for a system in the planning phase. Several institutes and companies currently work on the development of suitable models, algorithms (Berrian, 2017; Deline et al., 2013; Janssen et al., 2018; Reise and Schmid, 2015) and software (DiOrio and Deline, 2018; Kunath, 2017; Mermoud and Wittmer, 2017).

Considering the described limitations of the simulations a miniaturized test rig may be an interesting option in several regard. Provided that measurements of a miniaturized device can be assigned to the ones of a large test field, it can be used as cheaper and flexible testbed. Miniaturized devices could be used in long-term trials for on-site yield measurements of specific mounting situations, to identify optimum installation conditions or to validate simulation algorithms. The use of several test rigs with different configurations in parallel would additionally enable a direct comparison. The small size of a miniaturized rig also allows a fast change of the set-up, which is an interesting feature to test the respective impact at otherwise almost unchanged conditions in short-term tests. While a large PV system delivers important results in continuous long-term measurements, the manual change of the parameters will need some time due to the considerable dimensions. The idea to realize a miniaturized test rig resulted in a student work in which such a device was realized. It is a miniaturized version (Scale 1:12) of a test field which was already implemented on the roof of a ZHAW (Zurich University of Applied Science) building in Winterthur, Switzerland. This large test field consists of a 3 x 3 array of commercial 60-cell bifacial modules which, as a special feature, carries out a continuous and simultaneous rotation of all modules. Thus the effect of varied tilt angles at virtually identical insolation conditions can be analyzed. This corresponds to the simultaneous measurement of multiple arrays with different tilt angles but otherwise identical set-up; the same feature is realized in the miniaturized array.

In this paper we report about the measurement set-up and the comparison of the measurement data from the large and the miniaturized device. The measurement data of both systems is compared in order to investigate if there is a clear assignability. Irrespective of the planned application the assignability of the results to a real PV system with large modules is a prerequisite for a meaningful analysis with a miniaturized testbed. Because of the tilt angle variation the assignability of the measurements over the whole tilt angle range is tested. Based on the obtained data we give an estimation of the error in the prediction accuracy and discuss options for possible improvements.

According to our knowledge the approach to use a miniaturized test array is novel. As discussed, it is particularly useful for bifacial systems, for which a meaningful prediction accuracy with simulation tools is not possible yet.

2. Measurement set-up

At the ZHAW we implemented a 3x3 module array for the systematic measurements of bifacial systems with varying mounting conditions. The array is based on commercially available, 60-cell modules (Megacell MBF-GG60-270). Details to the array which is named BIFOROT (Bifacial Outdoor Rotor Tester) were presented earlier (Baumann et al., 2017; Klenk, 2016) .The basic set-up of the BIFOROT as well as of the miniaturized test rig is depicted in figure 1, the implemented large BIFOROT test rig is shown in figure 2. Three rows of modules with manually adjustable distance between the rows, are mounted on vertically adjustable pillars. The BIFOROT includes several features to analyze bifacial system properties, such as measurement of the rear side irradiation homogeneity, front and rear side measurements of bifacial modules (modules M1, M3 in figure 2) and others. The relevant device for this work is the bifacial module

in the center of the 3x3 matrix, marked red in figure 1 and labeled as M2 in figure 2. This module in the center module is best suited to reflect the shading situation for a typical location in an extended PV system. The benefit of the arrangement in form of an array, compared to more common test set-ups with stand-alone modules, is the similarity to real world installations with direct shading by other modules and indirect shading of the reflecting ground. Additional shading elements are applied to one side, a further extension in the large array was not feasible due to the limited available space on the roof of the building. Weather data and environmental conditions are recorded by several tools, such as pyranometers (horizontal and rotating with module front side), pyrheliometer, measurement of temperature, wind speed and rain, cloud camera and others.

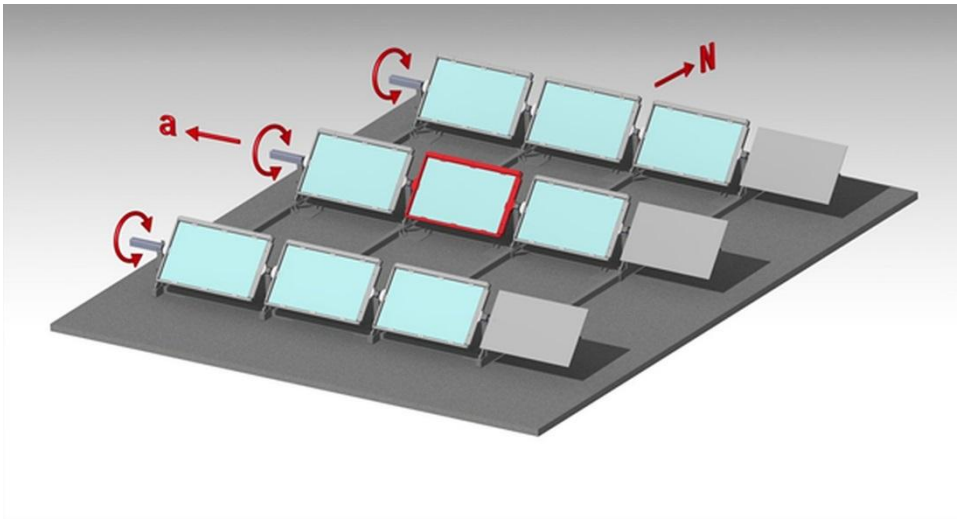

Fig. 1. Measurement setup with permanently turning modules. The most relevant module in the center, which is best suited to represent the actual conditions in real installations, is marked red.

A unique and central feature of the measurement set-up is the permanent variation of the tilt angle in steps (12 steps between 0 ° and 90 ° in one minute). All panels change their tilt angle coordinated with the central row. It is important to point out that the BIFOROT is no tracker, but a test system to compare the effect of different tilt angles at otherwise identical installation conditions. The impact of the tilt angle on the system performance is by far less straightforward for bifacial applications than for standard monofacial ones. The optimum tilt angle is dependent on height, albedo, location, irradiation conditions and the mutual shading due to other modules. Because of the permanent tilt angle variation the influence of this factor can be systematically investigated. The obtained results correspond to measurements of 12 systems in parallel with identical set-up, but varied tilt angle. This allows investigations such as the verification of simulation results for different irradiation conditions and tilt angles (Janssen et al., 2018; Klenk, 2018).

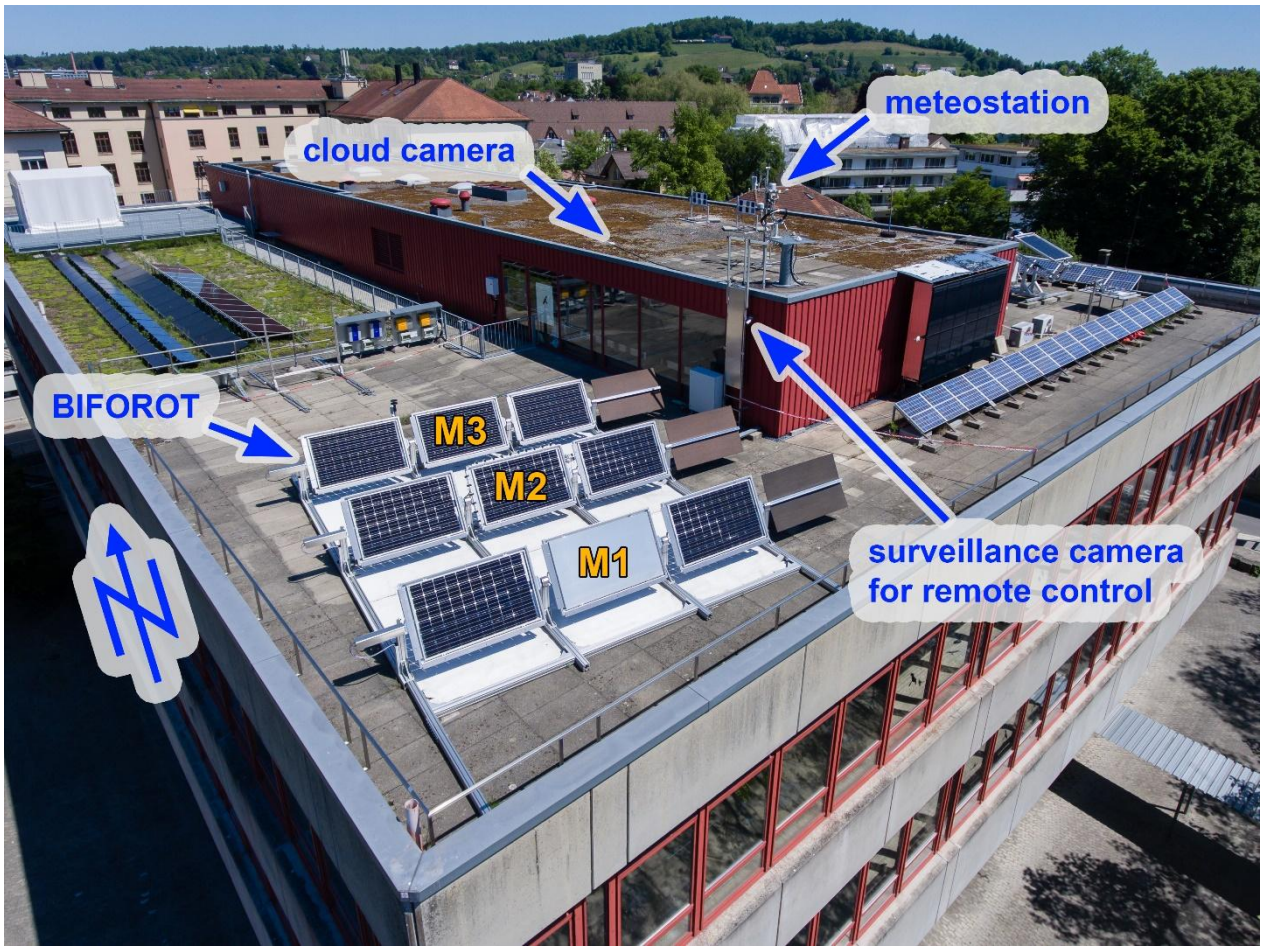

Fig. 2. BIFOROT installation on the roof of the ZHAW in Winterthur. White reflecting roofing foil is placed below the array.

The miniaturized test device is a small-sized replica of the large test array. A scale of 1:12 was chosen because the resulting dimensions still allow a fast manual adjustment of the mounting parameters. The same bifacial solar cells (n-Type, “BiSoN” cell type) as in the commercial 60-cell modules (Megacell, MBF-GG60-270) of the BIFOROT were used. In order to keep the proportions of real modules, bifacial solar cells were correspondingly cut to the size to obtain the same proportions, with one piece of solar cell representing the module area. Thus, the relative dimensions, such as the installation height over the ground, can be maintained. It should thus also be possible to analyze the impact of the installation conditions and their interrelation (height, albedo, tilt angle, row distance, and general orientation) for different irradiation situations.

Fig. 3. Miniaturized replica of the BIFOROT array with permanently turning mini-modules at 0 ° tilt angle. In this configuration the same white reflecting foil as in figure 2 is placed below the mini-modules.

Obviously not all parameters of a large system can be reflected by the miniaturized device, especially due to the fact that the solar cells will show a different behavior compared to full-scale solar modules, which are a series connection of multiple cells grouped in strings. This is particularly true for the response to direct shading, which typically results in the activation of the bypass-diodes in real modules. In later versions also smaller cell elements, representing cell strings or even smaller units in real modules, might be an option to overcome this limitation. Another difference is the used glass. In contrast to the miniaturized device glass of the large, commercial modules has an anti-reflective coating (ARC). It is well known that the effect is dependent on the angle of incidence. Even though particularly the tilt angle variation would therefore indicate to use the same glass type for both devices this was omitted, due to non-availability.

The tilt angle variation is synchronized for both test arrays, as exemplified in figure 4, and controlled by a LabView program. This LabView program also controls the IV-curve measurements of the central module in the BIFOROT as well as of the central solar cell in the miniaturized test rig. A set of load values is respectively adjusted to measure the IV-curves by an electronic load (Keysight N3305A, communication via Keysight 82357B interface). For the small test rig the cell voltage is increased by a constant voltage source to meet the system requirements.

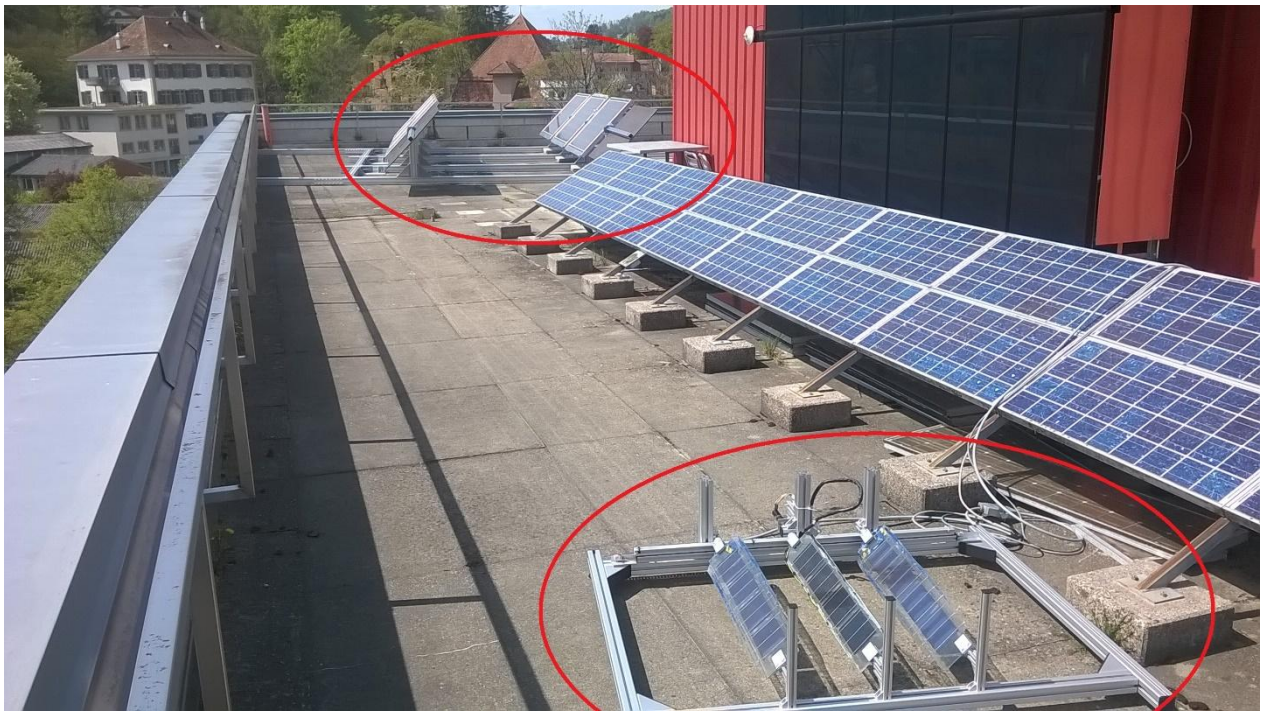

Fig. 4. Miniaturized array and BIFOROT on concrete ground. Both test rigs carry out a synchronized permanent tilt angle variation.

3. Objectives and methodology

As described in the introduction section miniaturized solar arrays may be an alternative to the use of simulation tools with still limited yield prediction accuracy for bifacial systems and an option to investigate bifacial-related issues in general.

Irrespective of the planned application it has to be shown that the measurement results of the miniaturized test device can be assigned to the one of the large PV system which is replicated. This is the central issue which is addressed in this work.

A miniaturized version of the existing BIFOROT test array is investigated in this regard. The results are however not limited to the specific lay-out of the BIFOROT, which acts as example for a typical system. Because of the synchronized variation of the tilt angle by both test rigs, the investigation is also expanded to the whole tilt angle range.

A suitable normalization or scaling is a prerequisite to assign measurement results of the small test rig to the ones of the reproduced large PV system. For the center module at the BIFOROT, as well as for the center cell at the miniaturized test rig, the nominal power at Standard Testing Conditions (STC) can be determined. As the same bifacial “BiSoN” solar cells are utilized in both devices their open circuit voltage should be the same as well as their temperature dependent cell properties. Their short circuit currents should reflect the respective active areas. For bifacial cells the use of the same or similar cell types is also important for the comparability because of the bifacial factor and the rear side. Even if the same cells are used, there will be deviating

fillfactor values for both systems, because of the differing contacting schemes. The ratio of the measured nominal powers represents a scaling factor at STC.

A scaling factor measured at STC can however not simply be assigned to other conditions than the ones at STC. Properties of both devices may show temperature, irradiation or tilt angle sensitive deviations. In order to reveal such effects the output of both test arrays is respectively compared and different options to define suitable normalization factors are analyzed.

The description and discussion follows the actual course of action in which experiments were carried out in form of comparative measurements. Basic properties are shown by a direct comparison of measurement data for a specific day and tilt angle. After verifying the normalization for a specific situation it is necessary to analyze the range of validity for a longer period of time. Such prolonged measurements include differing irradiation conditions and temperatures and should reveal potential drift effects. Due to the implemented tilt angle variation the analysis can be expanded to the whole tilt angle range. Based on the observed deviations and fluctuations a statement about the prediction accuracy is possible if the miniaturized test rig is used as a replacement for a real size system.

In order to perform comparative measurements both systems are arranged with the same global orientation (0 ° azimuth angle, south orientation). Both devices run in a synchronized manner with 12 tilt angle positions from 0 ° to 90 ° within one minute cycle time. At each position the IV-curves of the center module at the BIFOROT and of the center cell at the miniaturized array are recorded. During the period in which the reported experiments were carried out the BIFOROT performed a long-term measurement with unchanged installation conditions (row distance: 2.86 m, height of rotation axis: 0.75 m). Therefore also the corresponding parameters of the miniaturized version were kept constant for all comparative measurements as shown in this work (Scale 1:12). A further expansion of the measurement period with varied row distance, height and albedo would have been desirable, but the improvised character of the small test rig resulted in a breakdown which did not allow a continuation. The effects of installation height and row distance variation are however to a certain extend indirectly included in the experiments due to the tilt angle variation. For both systems a white roofing foil (manufacturer: Sika), as depicted in figures 2 and 3, was used to cover the ground during the whole reported measurement period. The white foil resulted in a measured albedo of 0.51 after several weeks in outdoor conditions.

4. Comparative measurements and discussion

Both devices run in a synchronized manner with 12 tilt angle positions from 0 ° to 90 ° within one minute cycle time. At each position the respective IV-curves and Pmpp values of the center module at the BIFOROT as well as of the center cell at the miniaturized array are recorded. For each of the two test rigs there are thus 720 Pmpp values per hour, with 60 Pmpp values per hour for each tilt angle position. The Pmpp values for both devices can be summed over the course of the day to obtain the daily yield. The miniaturized array with smaller area and deviating device lay-out obviously has a differing Pmpp output. In order to assign the data of the miniaturized array to the one of the large PV system a scaling has to be established.

In figure 5 the course of BIFOROT Pmpp values and scaled Pmpp values of the miniaturized device are exemplary shown for a day with mixed irradiation conditions and an arbitrarily selected tilt angle (2018/06/05; tilt 18 °). In this example the Pmpp data of the miniaturized array is multiplied with a single scaling factor which was selected to obtain the best match of both plots. The congruence in figure 5 is remarkably good, there is an almost complete concealing in the overlay of both plots.

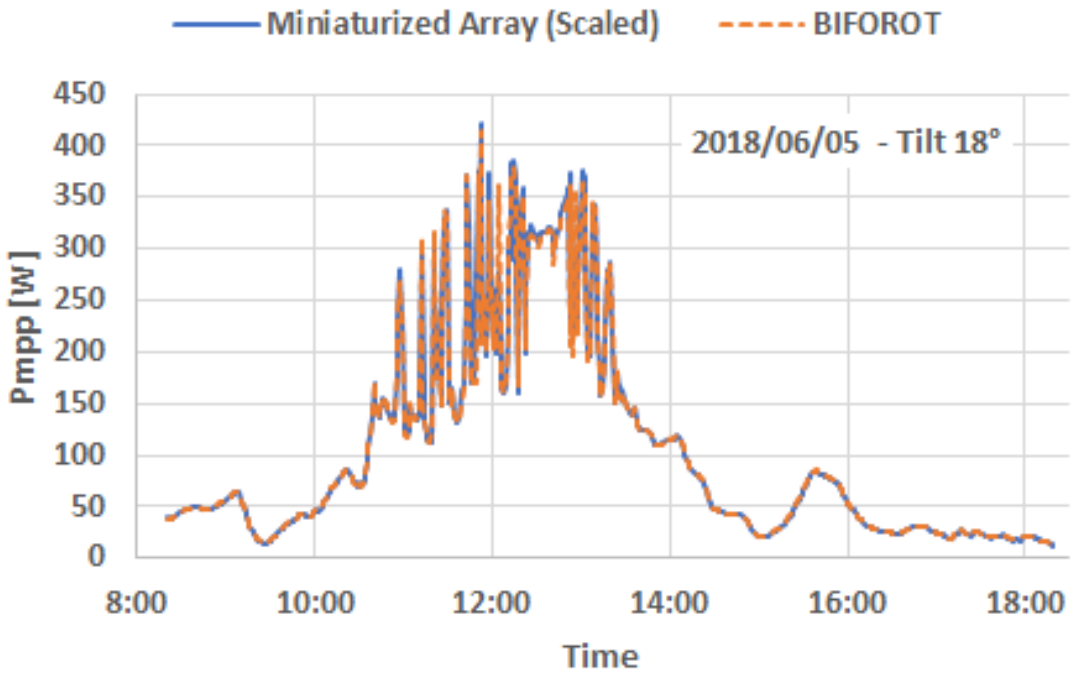

Fig. 5. The Pmpp values of the BIFOROT and the scaled Pmpp values of its miniaturized replica, plotted over the course of a day, show a remarkable congruence.

Corresponding results with similar congruence were obtained in numerous experiments. The congruence of the Pmpp data after applying a single scaling factor was quite surprising. Because of differing resistivity effects for both test rigs it was assumed that a suitable scaling includes temperature and intensity dependent factors to obtain a good congruence of the measurement data. Since there is an irradiation and temperature variation over the course of a day such temperature and irradiation related effects were expected for a plot as shown in figure 5. Apparently however, these effects are quite similar in both test devices. It has to be pointed out again that the same cell type was used in the miniaturized replica and the original array.

The encouraging results motivated a closer investigation of the prediction accuracy of a potential stand-alone test device. A prerequisite for this application is the determination of a scaling factor

or scaling procedure which allows an assignment of the miniaturized test rigs data to the real values of the original. The scaling factors, which were obtained in several similar experiments as visualized in figure 5, all had a value of about 140. This value is quite close to the active area ratio of both test rigs (12x12), as determined by the 1:12 scale, but showed small deviations. Because all measurements are subject to fluctuations also an analysis in this regard was carried out. This is exemplary visualized in figures 6 and 7 for a day (2017/05/09) with varying irradiance conditions and for 35 ° tilt angle. For each time stamp (60 time stamps / measurements per hour and tilt angle) the factor is determined which has to be applied to the Pmpp of the small device to obtain the Pmpp value of the BIFOROT. The resulting plot (figure 7) is well suited to visualize the distribution of the data. For a perfect congruence over the whole course of the day there would only be a single factor. In reality, with a certain distribution of the data, an average daily scaling factor can be determined. This average daily factor can then be used as a scaling factor for the small device which has to be applied to reproduce the output of the BIFOROT.

Figure 6 illustrates the congruence of the Pmpp plots from both devices after application of the average daily scaling factor as determined from the distribution plot in figure 7.

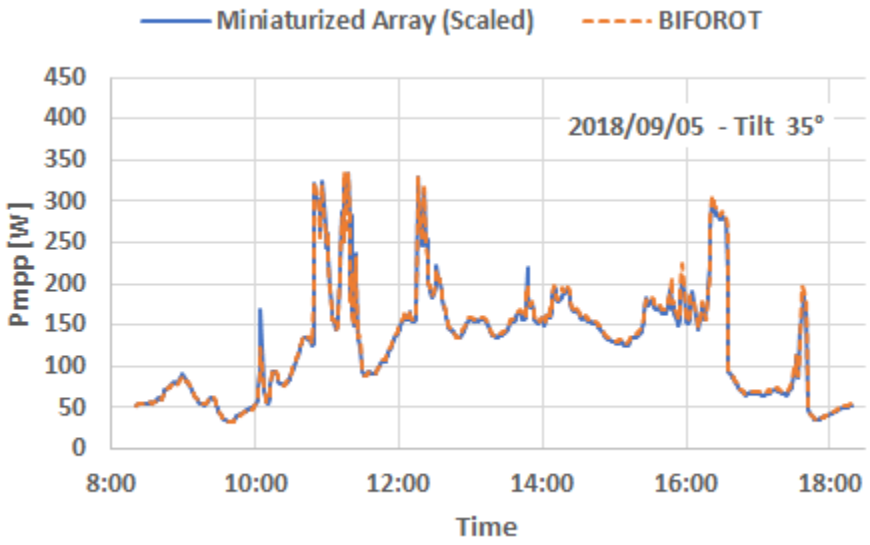

Fig. 6. Congruence of the Pmpp plots from both devices after application of the average daily scaling factor as determined from the distribution shown in figure 7.

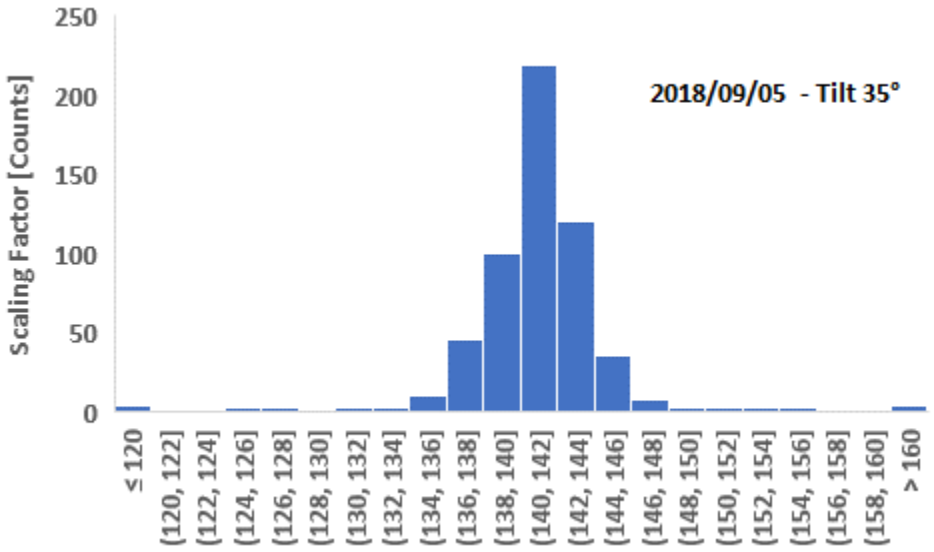

Fig. 7. For each time stamp in figure 6 there is a specific scaling factor. An average daily scaling factor can be determined by the distribution of all scaling factors for this day.

Quite similar averaged scaling factors were found if the same procedure was carried out for other tilt angles. This is exemplary shown in figure 8 for the same day as in the figures 6 and 7, but for four additional tilt angles, which include the whole range from 0 ° to 90 °.

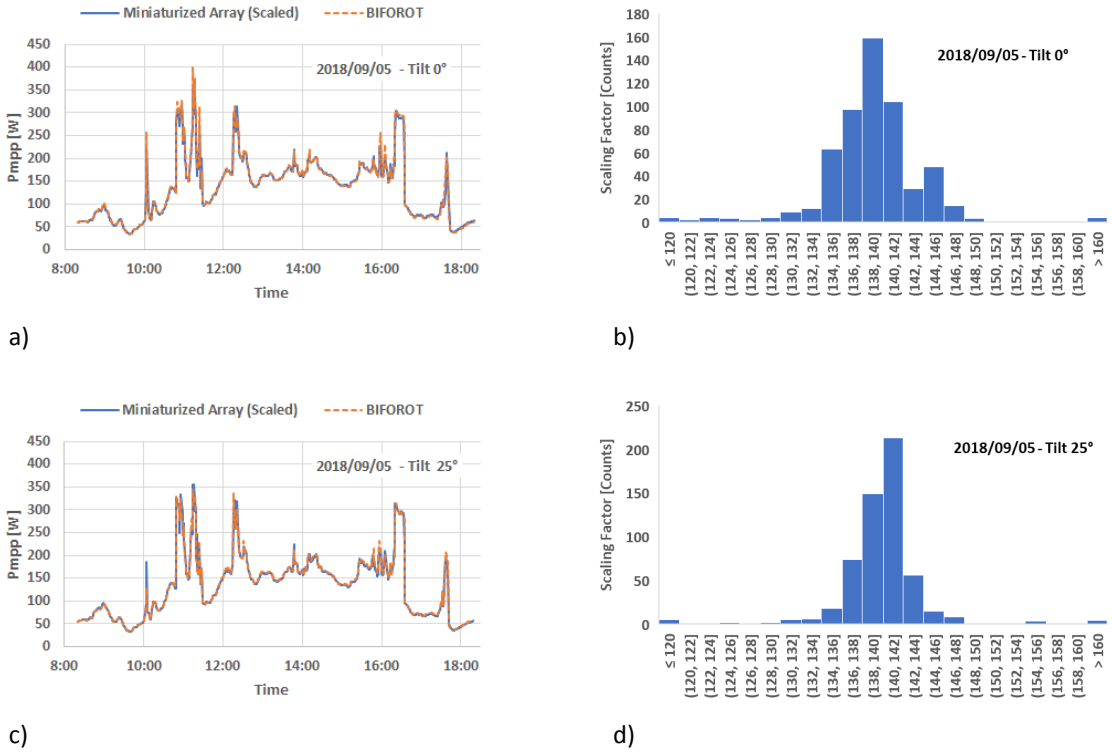

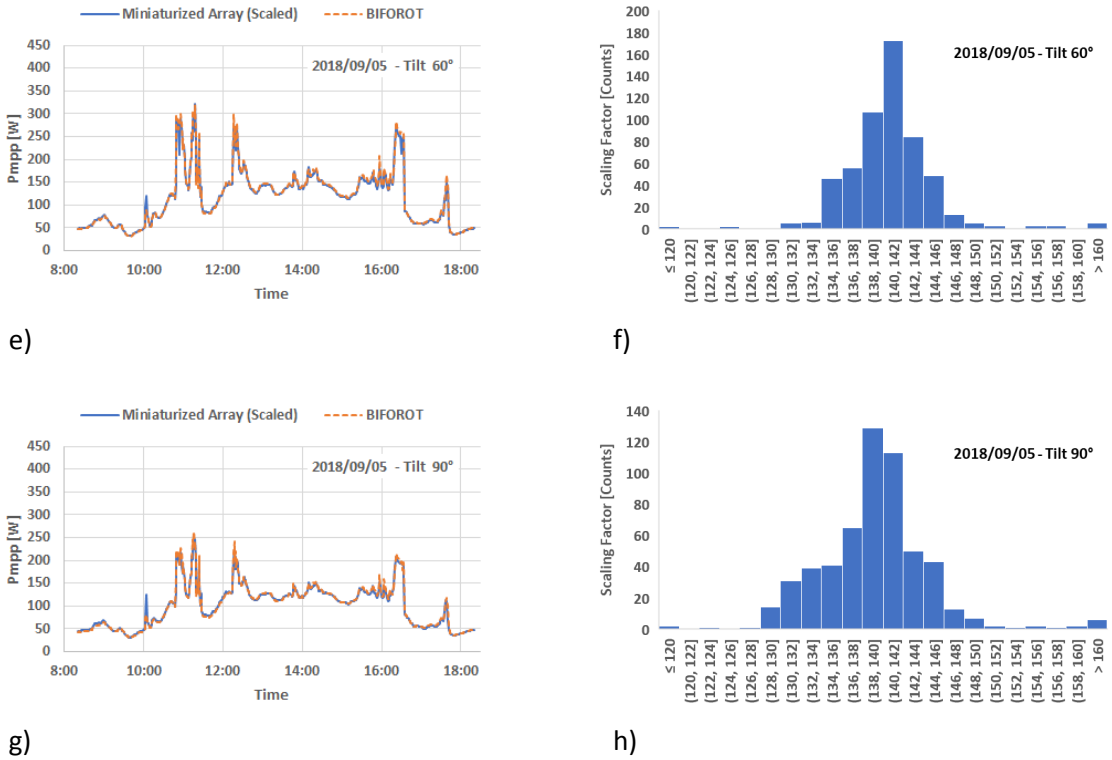

Fig. 8. BIFOROT Pmpp measurement data and scaled Pmpp data of the miniaturized array, again for the 2018/09/05 as an exemplary day, and for another four of the twelve tilt angles (left side). The average daily scaling factor is the mean value of the scaling factors for each time stamp, as respectively indicated on the right side.

The described line of action was expanded to a longer period of time in order to reveal potential drift effects and to investigate the long-term stability of the scaling factors for multiple days with varying temperature and irradiation conditions. Unfortunately, the improvised character of the small test device, which was not really well suited to prolonged exposure to outdoor conditions, resulted in a comparatively frequent down time and finally in a termination of the trials due to technical issues. While in some cases the operation was stopped for several days in other cases there was an interruption for hours. The frequent maintenance work caused again more issues such as unwanted variations of the global orientation. Nevertheless it was possible to obtain a data set with reliable data over a certain period of time from end of February to early May 2017. As described earlier the BIFOROT test array carried out long-term measurements with unchanged mounting conditions (albedo, axis height, row distance) during the whole reported measurement period. Accordingly also the parameters of the miniaturized rig were kept constant.

The proceeding as shown before in the figures 6 to 8, results in a descriptive picture of the scaling factor distribution. In the long term experiment we used however a similar but slightly different approach to determine the daily scaling factors, which were calculated as follows

$$\text{daily scaling factor} = \frac{\int \text{Pmpp}_{\text{BIFOROT}}\,dt}{\int \text{Pmpp}_{\text{Miniaturized Array}}\,dt}. \quad (1)$$

With this approach each daily scaling factor represents the factor which leads to a 100 % accordance of the daily yields from both test rigs for this day. The variation of this factor can therefore be interpreted as the measurement uncertainty for the comparison of both systems.

Due to the mentioned downtimes and interruptions rules had to be applied to ensure the comparability. Because we wanted to avoid an individual picking and appraisal of data points we defined rules for automated data selection. The first rule ascertains that the measurements of both devices start and end at the same time. The measurement that ends first or starts later is respectively taken as reference point for both devices. Missing data intervals due to downtimes, either from the miniaturized or the large test rig, are cut out in the other dataset as well. The third rule checks if there is a joint measurement time of at least six hours. If not, this day is left out.

As an example for the long-term trials the resulting plot of the daily scaling factors for the 0 ° tilt angle is shown in figure 9. The start and the end dates are respectively highlighted; the data points are also indicated by the vertical lines to improve the assignability to the measurement date. The general course is quite smooth, however with two distinct outliers, highlighted in figure 9. The mean value is in the expected range of about 140. There is no indication for temperature and irradiation dependent effects on the scaling factor during the observed period with varying daytime temperatures and zenith angle. Such slower changing parameters could as well result in a slope as a drift of the measurement hardware. Also an analysis of the data with regard to the daytime temperature and irradiation showed no indication for a correlation.

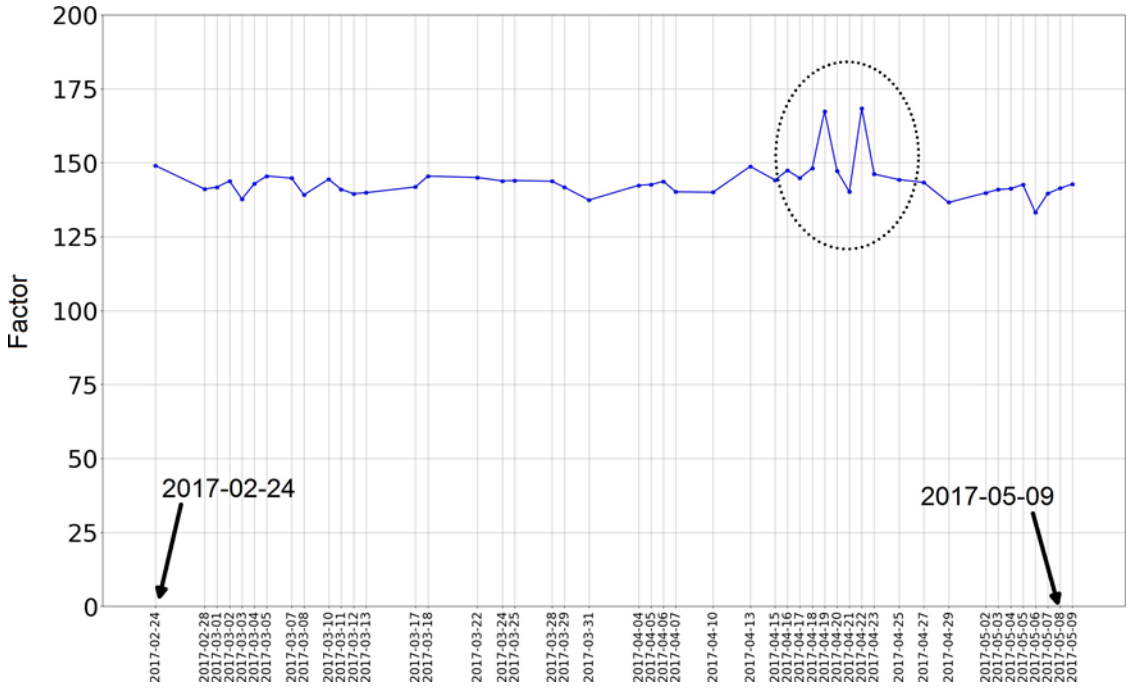

Fig. 9. Plot of the daily averaged scaling factor for 0 ° tilt angle. The start and end date are respectively highlighted; data points are also indicated by the vertical lines to enhance the visibility.

The constancy of the scaling factor and the insensitivity to ambient parameters (temperature, irradiation, zenith position) is promising with regard to the use of the miniaturized array as stand-alone test device. Determination of an applicable scaling procedure to reproduce the data of a large test field is a prerequisite and applying a single scaling factor is the simplest option.

By an averaging of the scaling factor data from figure 9 measurement fluctuations can be considered. However, the two distinct peaks in figure 9 obviously have an impact on the mean value of the scaling factor. In both cases the origin of the peaks was of similar appearance, and due to effects which we assigned to problems of the measurement equipment. Figure 10 shows a comparing plot of the Pmpp from both devices for one of the two distinct peaks. After 10 o´clock there is a sudden drop of the small rigs output. Directly before and after the sudden drop the data from both devices follows the same course with virtually identical short-term fluctuations, but with an off-set prior to and after the drop. Due to the same short-term fluctuations, apart from the offset, passing clouds or comparable ambient factors are not plausible. The origin of this effect could not be clearly identified, but a closer investigation is also not in the focus here. Instead this sudden drop is used as an example for specific events which are detrimental to the accuracy and which could be of different origin.

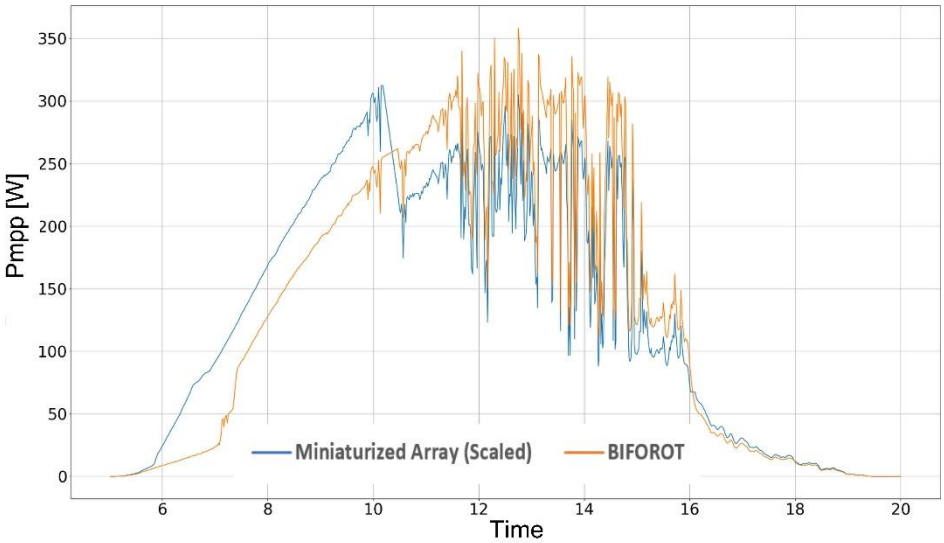

Fig. 10. Pmpp data for one of the two distinct peaks which are highlighted in figure 9. Shortly after 10 o´clock there is a sudden drop of the small rigs output.

While a definition of further rules to include comparable situations as in figure 10 may be possible in principle, also suitable mathematical measures can be chosen to suppress the impact of outliners. It was already pointed out that an individual appraisal of data points is

undesirable for a stand-alone test rig and erroneous data should be considered in an automated way.

In figure 11 the normal probability plot of the data from figure 9 is shown. This kind of plot visualizes if the data has a normal distribution and if the calculation of a mean value and standard deviation is meaningful. The norm quantiles are chosen to approximate the normal distribution. Data points outside of the dotted lines are incompatible to the assumption of a normal distribution. The graph indicates outliers and shows that the distribution of the factors is not perfectly normal. It backs however the assumption that the data is predominantly normally distributed and that grave outliners can be considered as caused by specific events, such as measurement artefacts. The numbered data points in figure 11 (upper right corner) represent the two distinct peaks.

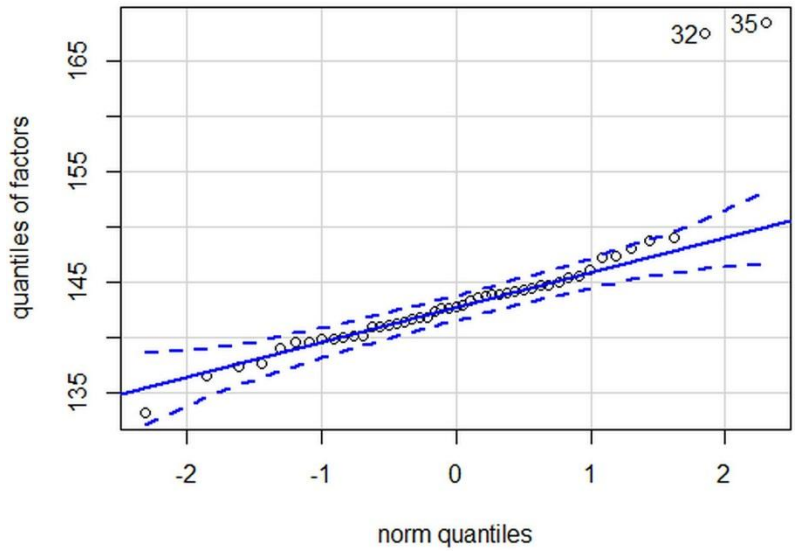

Fig. 11. Normal probability plot of the average daily scaling factors for the data as shown in figure 8 for 0 ° tilt angle. The numbered data points represent the two distinct peaks.

A means to suppress outliers in corresponding calculations is for example the application of the Huber M-estimator. It suppresses data points which do not match to otherwise normally distributed data sets. To demonstrate the effect of the Huber M-estimator it is applied on the data which is shown in figures 9 and 11. The results of the comparison are shown in table 1. In order to allow a comparison of the results, the mean value and the standard deviation is also calculated for the same data, but without the data points which correspond to the two distinct peaks. The differences are small, which indicates that this approach is well suited to minimize the impact of data which deviates from normally distributed data. Such deviating data is considered to be due to specific events such as measurement artefacts or ambient conditions which only affect one of both devices.

Scaling factor	Mean value	Standard deviation

Data as in figure 9	143.6	6.1
Data as in figure 9 but with the two distinct outliners removed	142.6	3.3
Data set as in figure 9 after application of the Huber M-estimator	142.8	3.3

Table 1: Mean value and standard deviation of the daily correlations factors as obtained from the data-set in figure 9 and after applying the Huber M-Estimator.

A corresponding analysis was carried out for all tilt angles and for the whole long-term measurement period. In table 2 there is a summary of the results for all twelve tilt angles after application of the Huber M-estimator.

Tilt angle [°]	Mean of the daily scaling factors with Huber M-estimator	Std.Dev. with Huber M-estimator	Std.Dev. with Huber M-estimator to mean [%]	Standard error of the mean (SEM)	SEM to mean [%]
0	142.8	3.3	2.3	0.34	0.23
10	144.3	3.1	2.2	0.32	0.22
15	144.8	4.2	2.9	0.42	0.29
18	144.8	4.4	3.0	0.44	0.30
21	145.0	4.0	2.8	0.41	0.28
25	144.9	4.3	3.0	0.44	0.30
30	145.3	4.2	2.9	0.42	0.29
35	145.5	4.0	2.8	0.41	0.28
40	145.6	5.2	3.5	0.51	0.35
45	145.6	5.2	3.6	0.53	0.36
60	147.5	7.3	4.9	0.71	0.48
90	143.8	9.2	6.4	0.93	0.65

Table 2: Scaling factor results, for all twelve tilt angles and the whole long-term measurement period with 47 measurement days (figure 9), after application of the Huber M-Estimator to reduce the impact of outliers.

The standard deviation is an index for the precision, which describes the fluctuation range of the measurements. According to table 2 the relative standard deviation is particularly low for lower tilt angles and if outliers were considered as described.

While the precision is a measure for the random fluctuations the accuracy represents the systematic deviation from the true value. The data points, measured over several days, show approximately a normal distribution (figure 11). Therefore there is an optimum scaling factor for each tilt angle, which is the mean value of the daily factors. The quality of the mean value estimation over several days can be expressed by the standard error of the mean (SEM). It is a measure of the dispersion of sample mean values from subgroups around the “true” mean value. In an often used approximated form the SEM can be calculated by

$$s_{\bar{x}} = \frac{s}{\sqrt{n}}. \qquad (2)$$

$s_{\bar{x}}$: SEM (approximated)

n: amount of selected data points (days)

s: standard deviation of the selected data points

Since we are interested in a rough estimation, details, such as correction factors for a small amount of samples, are neglected here. The quality of the mean value estimation improves with increasing amount of data points. In our case it is therefore advisable to record the measurements for the correlation factor determination over a period of days until a sufficiently low SEM is obtained. Both measurement quantities for fluctuations, the SEM and the standard deviation, increase for steeper tilt angles. For the measurement period of 47 days the SEM is however considerably lower than the standard deviation due to random errors.

The comparison of the mean values for different tilt angles may indicate that there is a differing angular sensitivity of the large modules with anti-reflective coating and the small device without ARC. The effect is small, but should be tracked in potential future experiments with increased data-set. For now we presume that there is a fix correlation factor for each tilt angle, even though the small difference of about 3% between the largest and smallest scaling factor would also allow the use of a value within this range for all angles, if this is considered in statements about the prediction accuracy.

The suitability of a single and constant correlation factor for each tilt angle is not obvious. As already described we expected that we have to calibrate the miniaturized test array with regard to certain properties, particularly the light intensity and temperature, when we started the experiments. Surprisingly, we found no significant effect of these parameters, which is reflected

by the demonstrated congruence of the signals during the course of a day with varying light intensity and temperature (figures 6 to 8) and also the stability over days and weeks with changing conditions (figure 9, table 2).

Provided that a new version of the miniaturized test field will be available for future experiments the impact of other factors such as the albedo or the installation height on the scaling factor have to be tested. This was not possible in the experiment up to the breakdown of the system. During the long-term measurement the parameters were kept constant in order to match the unchanged BIFOROT conditions. As shown in table 2 there is a small tilt angle dependency of the scaling factor. With the measured data it cannot be clarified if the variation is due to the anti-reflective-coating or actually reflects a height related dependency. The insensitivity of the scaling factors to the irradiance however indicates that albedo and height should not cause a factor variation. Changed installation heights and albedo variations have an impact on the irradiation homogeneity and on the irradiation intensity at the rear side. Similar effects are also caused by changing irradiation situations, during a day or from day to day, for which however no effect is observed. With a new miniaturized test rig such dependencies could be tested directly by comparative measurements or indirectly by for example checking front and rear effects separately with respectively shaded sides. If dependencies are revealed it has to be checked if they can be considered by a theoretical model or by an empirical correction.

While the above discussion was focused on the assignability of the measurement results, the same considerations are valid for the prediction accuracy if the miniaturized rig is used as a replacement for a large PV system.

For a measurement device the stability is essential. With regard to the data plot as shown in figure 9 a constant scaling factor leads to a horizontal regression line, while a drift would result in a slope. For the observed measurement period there is no indication for a drift. Moreover, as in all measurement tools the sensor, which in our case is the solar cell in the small test rig, should be calibrated regularly to exclude drift effects.

The discussion of the measurement data assignability and stability, based on recorded data, implies that future measurements will show the same characteristics. Due to the statistical nature there is some room for interpretation concerning the actual prediction reliability of the small test array. In general considerations often 1σ, as determined by the standard deviation, is taken to express the measurement uncertainty. In our previously chosen example for 0 ° tilt angle this means that a future data point will be with a probability of 68 % ($1\ \sigma$) within a range of ± 2.3 % due to random error. If the probability is increased to 95 % ($2\ \sigma$) the range is doubled. These statements are valid for a single future data point, in our case one measurement day.

The error is considerably reduced if not single measurement points (days) but measurement periods are considered. In this case again a mean value with a lower deviation than that of the random errors can be derived. In principle again the same assumptions as before for the SEM of the scaling factor determination should be applicable. This means that not only the quality of the scaling factor, but also the accuracy of averaged daily yields over a period of time, will improve with increasing duration. According to our results a prediction accuracy, expressed by the standard deviation of the mean value, of better than ±1 % is therefore possible in principle.

4. Outlook

All of the described tests to analyze the correspondence with the large test array were carried out with the same set-up (row distance, height, albedo), because the large BIFOROT array performed a long-term measurement with unchanged installation conditions.

Even though the observed insensitivity of the scaling factors to the irradiance indicates that the variation of height and albedo should not lead to a factor variation, this should be proven, provided that a new version of the miniaturized test field will be available for future experiments. Also the impact of the row distance variation should be analyzed in more detail. The adjusted row distance of the BIFOROT in the long-term measurement, with 2.86 m distance between the rows axes, was comparatively large and suppressed shading effects, compared to more closer packed systems. On the other hand, potential means to replicate the conditions in real modules, such as smaller cell elements, which represent cell strings or even smaller units, were not implemented yet. An advantage of the miniaturized system is the flexibility and lower cost which may allow the experimental testing of concepts. An example is visualized in figure 12. In this concept two systems are used in parallel to directly reveal the effect of differing set-ups. While the depicted example indicates the use of two different reflecting grounds, all parameters (height, row distance, global orientation) may be varied. Such a system would enable a direct comparison at identical illumination conditions and could be placed as stand-alone system.

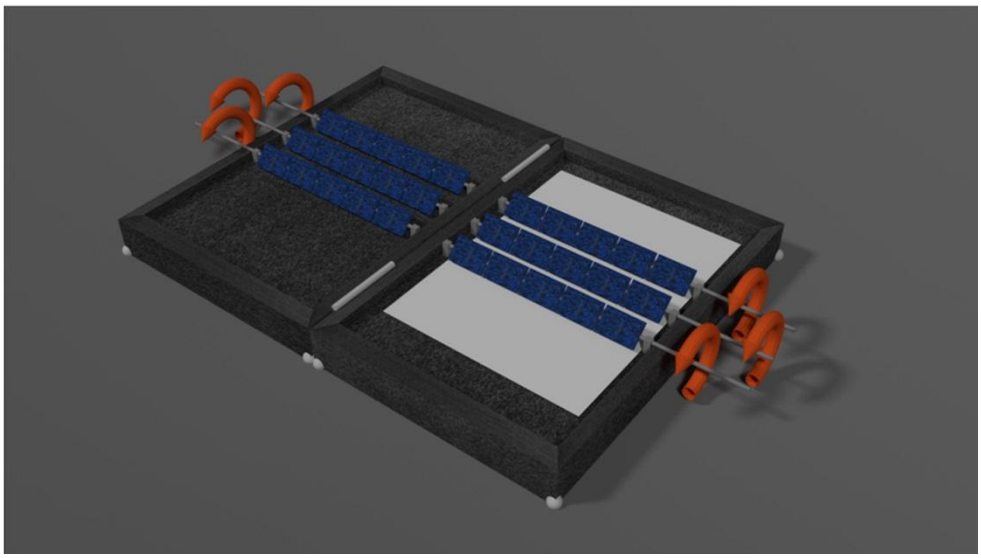

Fig. 12. Concept of a test device with two systems in parallel to directly reveal the effect of differing set-ups.

Another option beyond the use as yield prediction tool is the fast realization of different installation situations which allows a direct comparison. In earlier experiments we tested with the miniaturized array the effect of shaped reflectors in different lay-outs, as depicted in figure 13, on

the power output (Nussbaumer et al., 2016). Similar approaches to increase the yield of bifacial PV systems were in the meantime also suggested by others (Khan et al., 2018).

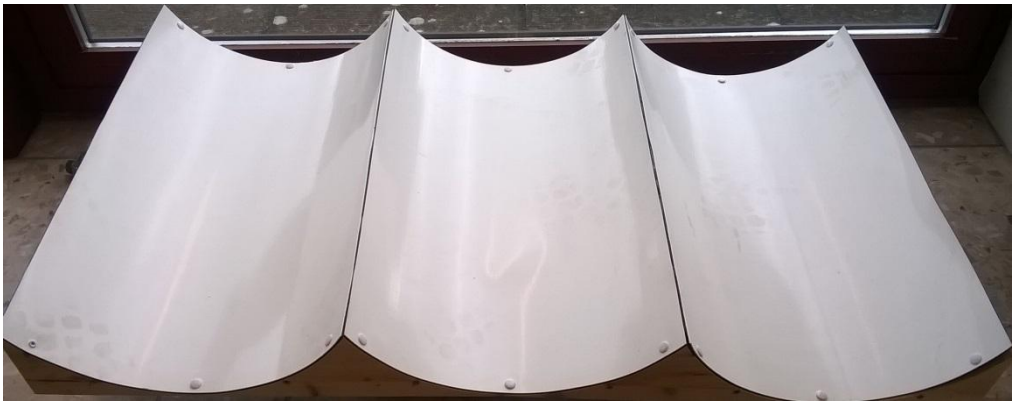

Fig. 13. Shaped diffuse reflector as placed below the miniaturized test array. The effect of such reflectors with different shape on the energy harvest is reported elsewhere (Nussbaumer et al., 2016).

5. Summary

It was possible to demonstrate that the output of a miniaturized replica can be assigned to the one of a real PV system. Due to a unique property of both testbeds, a continuous and coordinated variation of the tilt angle, the validation of the assignability is expanded to the whole angle range and potential dependencies are revealed. The assignability of the measurement enables several options for a potential application of the small array. First, it may be used as a flexible substitutional tool to determine the yield of planned PV systems by measurements within an available time frame. Furthermore the device allows the variation of different installation parameters to find the optimum for specific conditions in a comparative measurement set-up. Especially the optimum tilt angle is found for a given lay-out by the continuous, automated variation of this parameter. Other parameters, such as the height or the reflecting ground may be adjusted manually or automatically in order to analyze the effect of their variation.

Another option is the direct comparison of similar miniaturized systems with differently adjusted parameters which are used in parallel. Due to the smaller dimensions and the lower cost also the use of similar systems at different locations is feasible. The option of a fast variation of the installation parameters also allows a direct comparative analysis at virtually identical lighting conditions. So the effect of different reflective grounds, height variations or other changes may be recorded in fast adjacent measurements.

A relation between the large PV system and its miniaturized replica can be established with a scaling factor, which turned out to be independent on temperature and irradiation conditions. The accuracy with regard to the obtainable correspondence between a large PV system and its

miniaturized replica is surprising, particularly if extended measurement periods are considered. For single day and short-term measurements there are deviations (1σ) in the range of ± 2% to ±6.5%, dependent on the tilt angle. Due to the normally distributed data a mean value can be determined with improving accuracy for extended measurement durations. For the presented long-term measurement period a standard deviation of the mean value (SEM) below ± 1% was obtained. The same accuracy can be expected if a miniaturized system is used as a stand-alone test device to predict the output of a large PV system. The tests with the first version of the system had to be stopped because of the improvised nature of the device which finally led to a breakdown. Within the available time frame for the comparative measurements the large PV system carried out a long-term trial with unchanged height, albedo and row distance. Accordingly, also the parameters of the miniaturized system were kept constant, apart from the continuous and synchronized variation of the tilt angles. The assignability of the scaling factor to set-ups with other installation parameters still has to be proven, however the insensitivity to changing irradiance conditions is very encouraging in this regard.

The extremely promising results motivate the construction of a newtest array which should enable a more stable data collection and the implementation of technical improvements. Examples for such improvements could be the use of multiple elements, instead of a single solar cell, to represent cell strings in the modules or the application of the same anti-reflective coating on the front glass of both devices.

References

Baumann, T., Klenk, M., Keller, N., Nussbaumer, H., Baumgartner, F.P., 2017. Illumination Homogeneity of Bifacial Systems – Outdoor Measurements with Systematically Varied Installation Conditions. 33rd Eur. Photovolt. Sol. Energy Conf. Exhib. 1605-1609. https://doi.org/10.4229/eupvsec20172017-5bv.4.28

Berrian, D., 2017. MoBiDiG simulations and LCOE. Bifi PV workshop, Konstanz, Germany. http://bifipv-workshop.com/fileadmin/layout/images/Konstanz-2017/4__D._Berrian_ISC_KONSTANZ_MoBiDiG.pdf

Buchholz, F., Preis, P., Chu, H., Lossen, J., Wefringhaus, E., 2017. Progress in the development of industrial nPERT cells. Energy Procedia 124, 649–656. https://doi.org/10.1016/j.egypro.2017.09.276

Castillo-Aguilella, J.E., Hauser, P.S., 2016. Multi-Variable Bifacial Photovoltaic Module Test Results and Best-Fit Annual Bifacial Energy Yield Model. IEEE Access 4, 498–506. https://doi.org/10.1109/ACCESS.2016.2518399

Chiodetti, M., 2015. Bifacial PV plants: performance model development and optimization of their configuration. Master of Science in Energy Engineering-Energy technology, KTH Royal Institute of Technology

Colville, F., 2018. Bifacial bankability metrics need to shift from module maker to mounting provider [WWW Document]. PV Tech. URL https://www.pv-tech.org/editors-blog/bifacial-bankability-metrics-need-to-shift-from-module-maker-to-mounting-pr

Colville, F., 2017. Mono based PERC modules to drive bifacial market entry in 2018 [WWW Document]. PV Tech. URL https://www.pv-tech.org/editors-blog/mono-based-perc-modules-to-drive-bifacial-market-entry-in-2018

Deline, C., Dobos, A., Janzou, S., Meydbray, J., Donovan, M., 2013. A simplified model of uniform shading in large photovoltaic arrays. Sol. Energy 96, 274–282. https://doi.org/10.1016/j.solener.2013.07.008

DiOrio, N., Deline, C., 2018. Bifacial simulation in SAM. Bifi PV workshop, Denver, USA. http://bifipv-workshop.com/fileadmin/images/bifi/denver/presentations/4__Diorio-_Modeling_with_SAM_bifiPV2018.pdf

Faturrochman, G.J., de Jong, M.M., Santbergen, R., Folkerts, W., Zeman, M., Smets, A.H.M., 2018. Maximizing annual yield of bifacial photovoltaic noise barriers. Sol. Energy 162, 300–305. https://doi.org/10.1016/j.solener.2018.01.001

Foehringer Merchant, E., 2018. As Bifacial Solar Modules Inch Toward the Mainstream, Equipment Makers Prepare [WWW Document]. URL https://www.greentechmedia.com/articles/read/bifacial-solar-modules-inch-toward-the-mainstream

Guerrero-Lemus, R., Vega, R., Kim, T., Kimm, A., Shephard, L.E., 2016. Bifacial solar photovoltaics – A technology review. Renew. Sustain. Energy Rev. 60, 1533–1549. https://doi.org/10.1016/j.rser.2016.03.041

Guo, S., Walsh, T.M., Peters, M., 2013. Vertically mounted bifacial photovoltaic modules: A global analysis. Energy 61, 447–454. https://doi.org/10.1016/j.energy.2013.08.040

ITRPV roadmap, 2018. , International Technology Roadmap for Photovoltaic (ITRPV). http://www.itrpv.net/Reports/Downloads/

Janssen, G.J.M., Burgers, A.R., Binani, A., Carr, A.J., Van Aken, B.B., Romijn, I.G., Klenk, M., Nussbaumer, H., Baumann, T., 2018. How to Maximize the kWh/kWp Ratio: Simulations of Single-Axis Tracking in Bifacial Systems. 35th Eur. Photovolt. Sol. Energy Conf. Exhib. 1573-1577. https://doi.org/10.4229/35theupvsec20182018-6bo.7.5

Joanny, M., Libal, J., Kopecek, R., Veschetti, Y., Colin, H., 2017.Bifacial Systems Overview. Bifi PV workshop, Konstanz, Germany. http://bifipv-workshop.com/fileadmin/layout/images/Konstanz-2017/1__M._Joanny_INES_System_overview.pdf

Khan, M.R., Sakr, E., Sun, X., Bermel, P., Alam, M.A., 2018. Ground sculpting to enhance vertical bifacial solar farm output. ArXiv180606666 Phys.

Klenk, M., 2018. Bifacial modeling with the BIFOROT. Bifi PV workshop. Denver, USA. http://bifipv-workshop.com/index.php?id=denver-2018-program

Klenk, M., 2016. Bifacial Outdoor Rotor Tester- BIFROT. Bifi PV workshop. Miyazaki, Japan. http://bifipv-workshop.com/fileadmin/images/bifi/miyazaki/presentations/7_2_1-_KLENK_-_Biforot.pdf

Kopecek, R., Libal, J., 2018. Bifacial Photovoltaics: Technology, applications and economics, Energy Engineering Books. Institution Of Engineering And Technology. ISBN 978-1-78561-274-9

Kopecek, R., Veschetti, Y., Gerritsen, E., Schneider, A., Comparotto, C., Mihailetchi, V.D., Lossen, J., Libal, J., 2015. Bifaciality: One small step for technology, one giant leap for kWh cost reduction. Photovolt. Int. 26.

Kreinin, L., Bordin, N., Karsenty, A., Drori, A., Eisenberg, N., 2011. Experimental analysis of the increases in energy generation of bifacial over mono-facial PV modules, in: 26th European Photovoltaic Solar Energy Conference and Exhibition. Hamburg.

Kunath, L., 2017. Enhanced energy yield for PV systems using bifacial modules: simulation and model verification. Bifi PV workshop. Konstanz, Germany. http://bifipv-workshop.com/fileadmin/layout/images/Konstanz-2017/3__L._Kunath_POLYSUN_Enhanced_energy_harvest_simulation.pdf

Mermoud, A., Wittmer, B., 2017. Bifacial shed simulations with PVsyst. Bifi PV workshop. Konstanz, Germany. http://bifipv-workshop.com/fileadmin/layout/images/Konstanz-2017/2__B._Wittmer_PV_SYST_Bifacial_shed_simulations.pdf

Nussbaumer, H., Petrzilek, G., Schartinger, S., Klenk, M., Keller, N., Baumann, T., Carigiet, F., Baumgartner, F., 2016. Influence of Low Concentration on the Energy Harvest of PV Systems Using Bifacial Modules. https://doi.org/10.4229/EUPVSEC20162016-5BV.4.3

Obara, S., Konno, D., Utsugi, Y., Morel, J., 2014. Analysis of output power and capacity reduction in electrical storage facilities by peak shift control of PV system with bifacial modules. Appl. Energy 128, 35–48. https://doi.org/10.1016/j.apenergy.2014.04.053

Osborne, M., 2017. Black & Veatch and RETC to establish bifacial solar module rankings [WWW Document]. PV Tech. URL https://www.pv-tech.org/news/black-veatch-and-retc-to-establish-bifacial-solar-module-rankings

Reise, C., Schmid, A., 2015. Realistic Yield Expectations for Bifacial PV Systems – an Assessment of Announced, Predicted and Observed Benefits. 31st European Photovoltaic Solar Energy Conference and Exhibition; 1775-1779. 10.4229/eupvsec20152015-5co.14.6

Richter, A., 2018. An approach to quantify benefits & risks of bifacial PV systems based on energy yield. Bifi PV workshop. Denver, USA. http://bifipv-workshop.com/fileadmin/images/bifi/denver/presentations/3__Richter-_Benefits_and_risks_bifiPV2018.pdf

Romero, R., Kedir, C., 2018. Performance Analysis and Ranking of Bifacial Modules. Bifi PV workshop. Denver, USA. http://bifipv-workshop.com/fileadmin/images/bifi/denver/presentations/2__Romero-_bifacial_characterisation_program_bifiPV2018.pdf

Shoukry, I., Libal, J., Kopecek, R., Wefringhaus, E., Werner, J., 2016. Modelling of Bifacial Gain for Stand-alone and in-field Installed Bifacial PV Modules. Energy Procedia 92, 600–608. https://doi.org/10.1016/j.egypro.2016.07.025

Soria, B., Gerritsen, E., Lefillastre, P., Broquin, J.-E., 2016. A study of the annual performance of bifacial photovoltaic modules in the case of vertical facade integration. Energy Sci. Eng. 4, 52–68. https://doi.org/10.1002/ese3.103

Stein, J.S., Riley, D., Lave, M., Hansen, C., Deline, C., Toor, F., 2017. Outdoor Field Performance from Bifacial Photovoltaic Modules and Systems. https://www.osti.gov/servlets/purl/1457637

Sugibuchi, K., Ishikawa, N., Obara, S., 2013. Bifacial-PV power output gain in the field test using “EarthON” high bifaciality solar cells, in: Présenté à 28th European Photovoltaic Solar Energy Conference and Exhibition, Paris.

Sun, X., Khan, M.R., Deline, C., Alam, M.A., 2018. Optimization and performance of bifacial solar modules: A global perspective. Appl. Energy 212, 1601–1610. https://doi.org/10.1016/j.apenergy.2017.12.041

Teppe, A., Gong, C., Zhao, K., Liu, J., Wang, S., Dong, J., Zhou, S., Keller, S., Klenk, M., Melnyk, I., Fath, P., 2015. Progress in the Industrial Evaluation of the mc-Si PERCT Technology Based on Boron Diffusion. Energy Procedia 77, 208–214. https://doi.org/10.1016/j.egypro.2015.07.029